https://doi.org/10.3311/PPci.41796

Periodica Polytechnica Civil Engineering, 70(1), pp. 327–341, 2026

Combined Effects of Particle Shape and Deformability on Cyclic Shear Response of Sand-rubber Mixtures

Abdulmuttalip Ari[1*], Suat Akbulut[1]

[1] Department of Civil Engineering, Yildiz Technical University, Davutpasa Street, B-Block, 34220 Esenler, Istanbul, Türkiye
[*] Corresponding author, e-mail: talipari@yildiz.edu.tr

Received: 31 July 2025, Accepted: 16 March 2026, Published online: 25 March 2026

Abstract

In this study, the cyclic response of sand-rubber mixtures was investigated in terms of shape and deformability effects of particles. A series of cyclic simple shear tests were performed using three different sand and two different rubber specimens. The rubber particles were included in the sand samples with five different contents, and the mixtures were loaded until five different shear strain levels. The cyclic response was evaluated using secant shear modulus and damping ratio parameters. The particle deformability and shape effects of the rubber particles were elaborated using local images from the tests. In addition, the mixtures were subjected to California bearing ratio test to correlate the cyclic response with static behavior. The results were evaluated by adopting an interactive approach by considering the shape and deformability of the particles together. It was revealed that the influence of shape and rubber content on the cyclic parameters were found to be highly dependent on the shear strain level. The shear modulus at small strain levels followed similar trends as the bearing ratio in terms of particle shape and rubber content influences. The contribution of sand and rubber particles to the damping ratio varied with the shear strain, and particle shape effects emerged at large strain levels. The local image of the samples reveals that the response of the mixtures is transformed as the rubber particles produce primary force columns. Rubber particles can provide a fiber effect depending on the shape features.

Keywords

particle shape, particle deformability, sand, rubber, shear modulus, damping ratio

1 Introduction

The mechanical response of granular materials is affected by the physical condition of the particles. Particle morphology serves as a primary physical factor governing the mechanical behavior of granular assemblies [1–3]. In recent years, the use of rubbers from recycled tires in geotechnical engineering applications has attracted the attention of researchers [4–6]. The rubber particles have a superiority against sand particles in terms of energy absorbing features. This provides an advantage in geotechnical engineering for mitigating earthquake-related damage on the structures. Since rubber particles have a soft structure, unlike rigid sand particles, their particle shape can change depending on external loads. This complicates the role of particle shape on the behavior of mixtures. Therefore, a coupled approach that takes particle shape and deformability into account is needed to accurately understand the cyclic response of sand-rubber mixtures.

In the literature, the effect of particle shape on the monotonic shear response of sandy soils has been investigated for various experimental conditions [7–9]. However, studies examining the role of particle shape on the dynamic response are relatively limited. Shin and Santamarina [10] and Ha Giang et al. [11] observed that the small-strain shear modulus increased with the angularity of the particles. However, Sarkar et al. [12] and Ahmed and Martinez [13] stated that the small-strain shear modulus decreased with increasing angularity. Hu et al. [14] reported that the angular particles produced a higher secant shear modulus than the rounded particles, and the particle shape influence on the damping ratio appeared at relatively large strains. The global performance of granular assemblies is a direct consequence of the mechanical interactions occurring between individual particles at the local scale. These local contact dynamics essentially govern the overall evolution of the material's

Cite this article as: Ari, A., Akbulut, S. "Combined Effects of Particle Shape and Deformability on Cyclic Shear Response of Sand-rubber Mixtures", Periodica Polytechnica Civil Engineering, 70(1), pp. 327–341, 2026. https://doi.org/10.3311/PPci.41796

response. In the case of adding rubber to sand material, the role of particle shape on the mechanical response needs to be related to the change in particle deformability.

Researchers have investigated the effect of rubber particles on the dynamic behavior of mixtures for different rubber contents and different shear strain ranges. It is reported that the shear modulus decreases and the damping ratio increases with increasing rubber content [15, 16]. Previous studies have shown that the effect of rubber particles on the response can vary greatly depending on the level of shear strain. Madhusudhan et al. [4] observed an optimum rubber content in terms of maximum damping ratio at large shear strain. Furthermore, existing research indicates that soil-rubber mixtures exhibit optimal static and dynamic performance at specific replacement ratios, providing an effective seismic isolation solution for low-rise structures [17, 18]. Liu et al. [19] reported that there is a threshold shear strain value in terms of the effect of rubber addition on the damping ratio. Adding rubber increased the damping ratio when shear strain was lower than the threshold value. Edinçliler and Yildiz [20] studied the influence of rubber form on the cyclic response. It was stated that as the aspect ratio of the rubber particles increased, the shear modulus increased while the damping ratio decreased. Overall, the literature review reveals that researchers have attempted to study the response of the sand-rubber mixture in terms of the deformability effect of the particles. The role of particle shape has been largely ignored. This represents a significant gap, as the shape of both the sand and the rubber likely dictates how the particles behave together during cyclic loading. To accurately understand and predict the mixture's behavior, it is necessary to study the combined influence of both shape and deformability.

In this study, the cyclic response of sand-rubber granule mixtures was investigated in terms of particle shape and deformability effects. To this end, three different sand and two different rubber samples were prepared, and the particle shape features were digitized with a comprehensive shape parameter using the image processing technique. The experimental program involved blending rubber particles with the sand matrix at five separate weight-based percentages. The mixtures were tested using cyclic simple shear device under five different shear strains. The results were evaluated using the secant shear modulus and damping ratio parameters. Local images of the mixtures were taken to reveal in detail the impact of rubber particle shape and content on the behavior. In addition, California bearing ratio tests were conducted to relate the cyclic response of the mixtures to their static behavior.

2 Sand and rubber particles

In this study, three distinct sands and two different rubber particles were utilized. All samples were prepared in a single and similar grain size range to eliminate the influence of particle size on the response as shown in Fig. 1. The sample images for these particles are presented in Fig. 2. The particles were chosen by considering the shape properties of the materials. In sand samples, manufactured glass beads (S1) were used to represent the effect of super-regular particles on the cyclic response. The glass bead particles are intentionally manufactured to be spherical, exhibiting a near-ideal geometry with smooth surfaces. Consequently, they possess an exceptionally high degree of roundness that is rarely observed in natural granular materials. Therefore, the term super-regular is used to classify the S1 particles. Beach sand (S2) was used to accommodate a shape class between super-regular and irregular particles. Lastly, the role of irregular particles was reflected using crushed sand specimen with irregular particles (S3). The samples were classified as poorly graded sand (i.e., SP) according to Unified Soil Classification System (USCS).

For the part of rubber samples, crumb and elongated particles were used to include the shape effect. The rubber samples were supplied by a local firm. Crumb rubber particles (R1) were used as supplied by the company, but elongated rubber particles (R2) were deliberately prepared to achieve a more elongated form. R1 particles have the same particle size range as sand samples. However, the R2 particle width is in the range of 0.6–2.0 mm and the length is in the range of 4.0–7.0 mm; therefore, the grain size distribution curve measured from sieve analysis has a different trend from the other samples, as shown in Fig. 1. A series of tests was conducted to determine the index properties of the

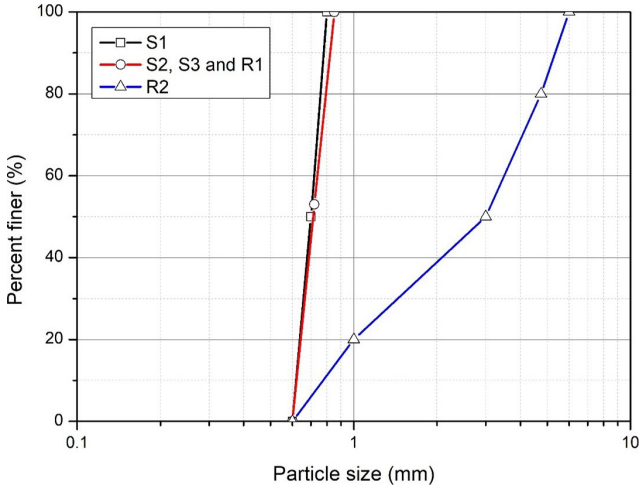

Fig. 1 Particle size distribution of sand and rubber particles

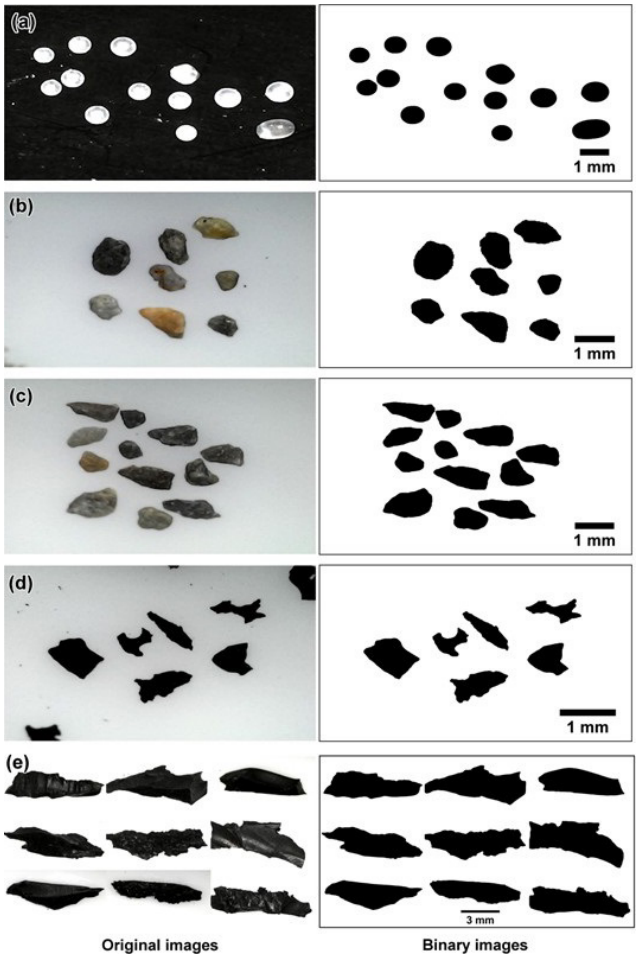

Fig. 2 Original and binary images of particles: (a) S1 sand; (b) S2 sand; (c) S3 sand; (d) R1 rubber; (e) R2 rubber

granular materials. The specific gravity of the samples was determined according to ASTM D854-23 standard [21]. Maximum and minimum void ratios of the sand samples were determined using standard Proctor compaction test method according to ASTM D698-12 standard [22]. The void ratios for the pure rubber materials (R1 and R2) were not determined using ASTM D698-12 standard [22] procedures, as the high elasticity of the rubber inhibit the attainment of a stable index density state. The index properties of the samples were presented in Table 1.

3 Particle shape classification

The particle shape of the sand and rubber particles was evaluated using three different aspects of particle geometry, namely aspect ratio (AR), convexity (C), and sphericity (S). These shape parameters are used to classify macro scale shape features of particles [23, 24]. AR is the ratio of minimum Feret diameter to maximum Feret diameter. C is calculated as the ratio of the projected particle area to the area of convex shape. S quantifies the degree of similarity

Table 1 Index properties of granular samples

Particle name	Mean particle size (D_{50}) (mm)	Specific gravity (G_s)	Maximum void ratio (e_{max})	Minimum void ratio (e_{min})
S1	0.70	2.50	0.76	0.57
S2	0.72	2.64	0.81	0.58
S3	0.72	2.65	0.87	0.60
R1	0.72	1.13–1.16		
R2	3.00	1.13–1.16		

between a particle and a sphere, calculated as the ratio of the perimeter of the equivalent circle with the same area as the particle, to the actual perimeter [25–27]. The mathematical definitions used in the calculation of these parameters are presented in Table 2.

The sand and rubber samples utilized in this investigation were deliberately selected based on their distinct formation histories for the sands and controlled mechanical shredding for the rubber particles. While the qualitative differences in shape (e.g., angular *vs*. rounded, crumb *vs*. elongated) were established by the material origins, a quantitative shape measurement was conducted to differentiate the samples mathematically. In the measurement of particle shape, image processing technique was utilized. For this purpose, firstly, a sample of 100 particles was randomly selected from each granular group for analysis. Established literature in geotechnical image processing has demonstrated that a sample size of 100 particles provides a sufficiently robust statistical basis to accurately classify the macro-scale shape features of sands and similar granular materials [28, 29]. To ensure a consistent and representative 2D characterization, each particle was manually oriented on its most stable facet prior to imaging. The particle images were obtained by a digital microscope with 30× magnification, as shown in Fig. 2 and then they were processed using ImageJ open-source software [30, 31]. In the image processing step, the original images were transformed to the binary form by applying thresholding to distinguish the particle outline from

Table 2 Mathematical definitions for shape parameters

Parameter	Formulation	Description
Aspect ratio	$\mathrm{AR} = \frac{D^{F_{min}}}{D^{F_{max}}}$	$D^{F_{min}}$: minimum Feret diameter $D^{F_{max}}$: maximum Feret diameter
Convexity	$\mathrm{C} = \frac{A}{A+B}$	A: real area of particle $A + B$: area of convex shape
Sphericity	$\mathrm{S} = \frac{2\pi R_e}{P_r}$	R_e: radius of circle having same area as particle P_r: perimeter of particle

background. The default method (i.e., Otsu algorithm) was used in the thresholding step. In order to evaluate the particle shape with a single quantitative parameter, Overall Regularity (OR) concept was applied as recommended by [23]. In this concept, OR includes comprehensive information on macro-scale shape features by combining AR, C, and S through the following definition (Eq. (1)):

$$OR = \frac{AR + C + S}{3}. \quad (1)$$

Figs. 3 and 4 show the statistics on the shape parameters of sand and rubber particles, respectively. The plots are box-and-whisker diagrams where the whiskers represent the full range (minimum and maximum) of the 100-particle dataset, the box represents the standard deviation, and the

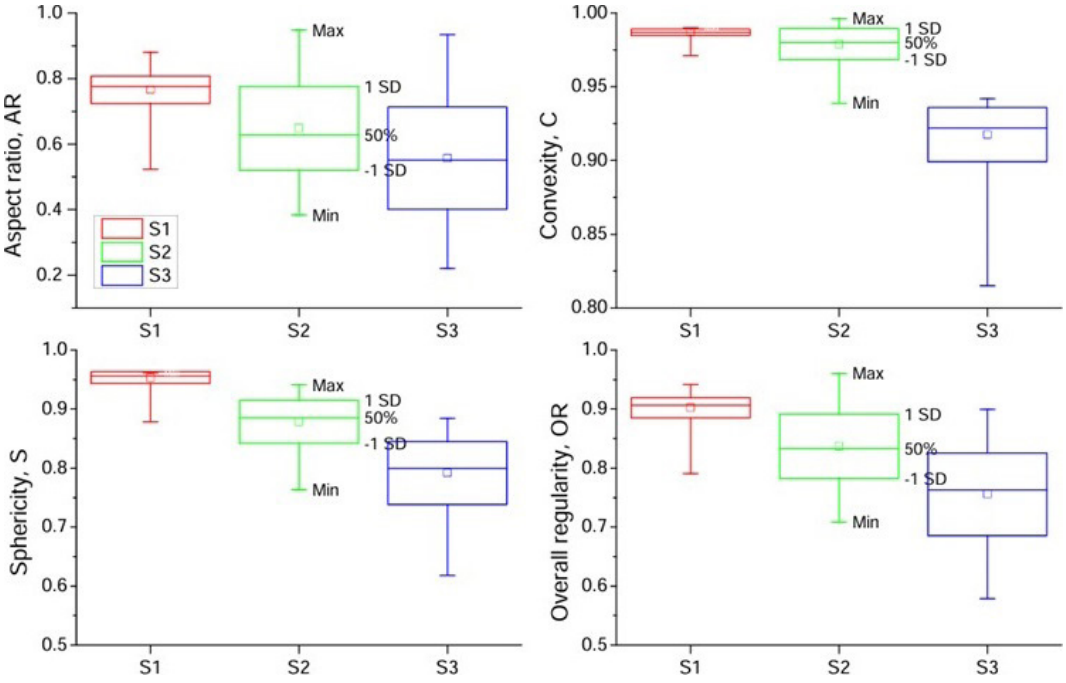

Fig. 3 Statistics on shape parameters of sand particles

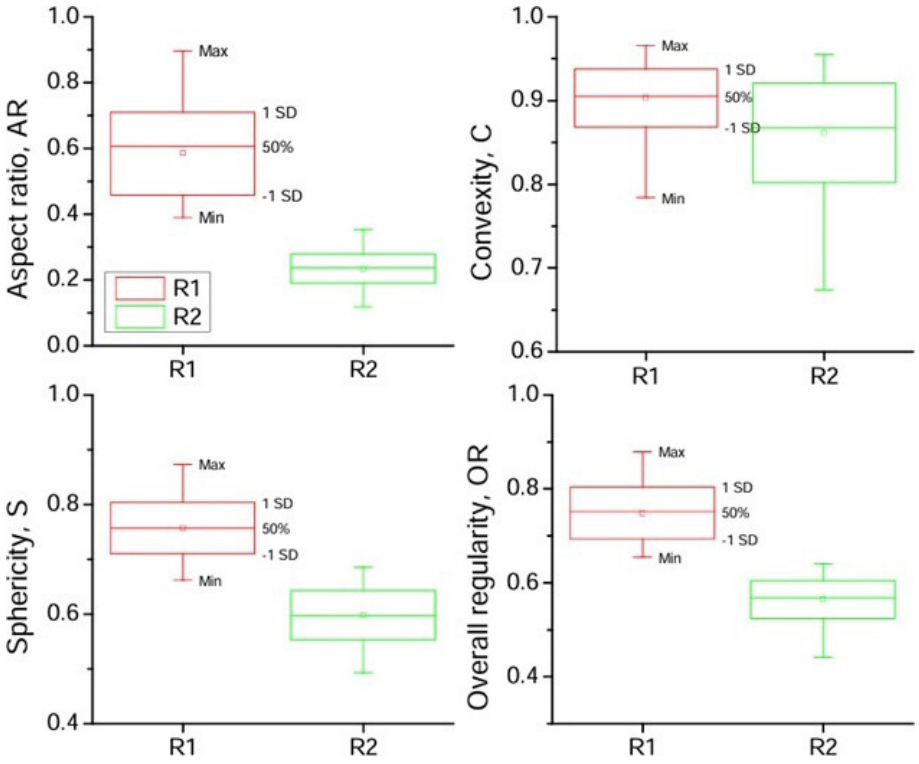

Fig. 4 Statistics on shape parameters of rubber particles

central markers indicate both the median (i.e., 50%) and the mean. Table 3 shows the mean values for the shape parameters. The mean OR values were considered as representative values for each particle group. The shape measurement showed that for both sand and rubber, particle groups produced distinct shape classes in terms of OR values.

4 Experimental program

In the experimental program, both the static and dynamic responses of the mixtures were investigated using different test methods.

4.1 California bearing ratio (CBR) test

In this study, CBR test was conducted to evaluate the effect of particle shape and deformability on the bearing capacity of the mixtures for static loading condition. While the rubber additives can improve the cyclic response, they can reduce the material's bearing capacity and increases the potential for settlement (static response). The incorporation of the CBR test serves to quantify the static performance of the mixtures, providing a baseline for bearing capacity and a practical assessment of settlement potential. This provides a clearer understanding of the practical limits of rubber additives in terms of overall geotechnical safety. The test was performed according to ASTM D1883-21 standard [32]. For this purpose, the samples were compacted into CBR mold with an inside diameter of 152 mm and a height of 178 mm. According to ASTM D698-12 standard [22], the maximum particle size should be less than 19.0 mm to ensure effective compaction. As shown in Fig. 1, the particle size distributions of the tested samples satisfy this requirement. The rubber content in the mixtures was arranged considering the total weight of the samples. The compaction process was done in 5 layers, and 37 blows were applied to each layer. The number of layers and blows were determined by considering the energy required to reach the compression level obtained from standard Proctor tests.

A surcharge load of 4.5 kg using metal weights was placed on the samples and CBR mold was positioned in the loading system. The CBR tests were carried out on the unsoaked samples. The samples were compressed with a cylindrical piston with a penetration speed of 1.27 mm/min. Finally, the variation of load with penetration of piston was recorded during the tests. Table 4 shows the testing program for the different sand-rubber particle combinations.

Table 3 Mean shape values for sand and rubber

Particle	AR	S	C	OR
S1	0.766	0.958	0.987	0.904
S2	0.649	0.878	0.979	0.837
S3	0.558	0.792	0.918	0.756
R1	0.585	0.757	0.903	0.748
R2	0.234	0.598	0.861	0.564

4.2 Cyclic simple shear test

In geotechnical engineering, several laboratory tests are employed to characterize the cyclic response of granular materials. The selection of the appropriate apparatus is primarily governed by the targeted shear strain amplitude. The cyclic response in the small strain tests are generated elastic vibration of particles within a stable fabric [33]. Because this study aims to investigate how particle shape and deformability influence energy dissipation and stiffness, it is necessary to induce more significant mechanical responses, including sliding, rolling, and particle rearrangement [34]. Such movements generate inherent volume change tendencies (contraction or dilation) that are characteristic of the medium-to-large strain level. Therefore, the sand-rubber mixtures were aimed to shear under medium-to-large strain levels [17]. In this study, a Geocomp ShearTrac II, which is a Norwegian Geotechnical Institute (NGI) type simple shear device, was used in cyclic tests. The NGI type simple shear device was originally pioneered by Bjerrum and Landva [35] to investigate the undrained shear response of Norwegian quick clays. The primary motivation for its development was the need to overcome the limitations of the traditional direct shear box, which suffered from non-uniform stress distribution and a forced failure plane. Over the following decades, the application of the simple shear test expanded beyond clays to become a benchmark for evaluating the cyclic response of granular materials [36]. This setup maintains a K_0 (at-rest) condition during consolidation, which preserves the fabric of the compacted mixture better than the isotropic consolidation typically used in triaxial testing. In addition, unlike the cyclic triaxial test, which involves an abrupt 90° rotation of principal stresses, the simple shear allows for a smooth and continuous rotation of principal stress axes. This more accurately replicates the stress conditions experienced by a soil element during a cyclic loading [37]. Despite its advantages in simulating principal stress rotation, the shear stress is only applied to the horizontal planes (top and bottom) and the stress distribution within the specimen is not perfectly uniform.

The device has a fully automatic system for applying vertical and horizontal loads and recording the relevant

displacements. An overall view of the test setup is presented in Fig. 5 (a). The densest packing conditions were targeted in the preparation of the samples. Therefore, the sample mass for each rubber content was decided considering the maximum dry unit weight of the mixtures, as shown in Fig. 6. The maximum and minimum dry unit weights of the mixtures were determined using ASTM D4254-00 [38] and standard Proctor compaction (ASTM D698-12 [22]) tests, respectively. Fig. 6 shows that the dry unit weights decrease with increasing rubber contents. The required amounts of sand and rubber particles were first weighed based on the target rubber content and mixed thoroughly to ensure a uniform distribution of rubber particles within the sand matrix. The mixtures were compacted homogeneously in four consecutive layers and samples with a diameter of 63 mm and a height of 20 mm were prepared as shown in Fig. 5 (b). The lateral confinement for samples was provided by a stack of teflon coated aluminum rings around a latex membrane (Fig. 5 (c)). According to ASTM D6528-24 [39], the maximum particle size should be less than one-tenth of the specimen height. In this study, the particle sizes of the sand samples satisfy this requirement. In addition, since the elongated R2 rubber particles may have larger characteristic dimensions compared to the sand particles, the content of R2 rubber in the mixtures was limited to a maximum of 10% to minimize potential scale effects. Table 4 shows the testing program for different shape of sand and rubber particles.

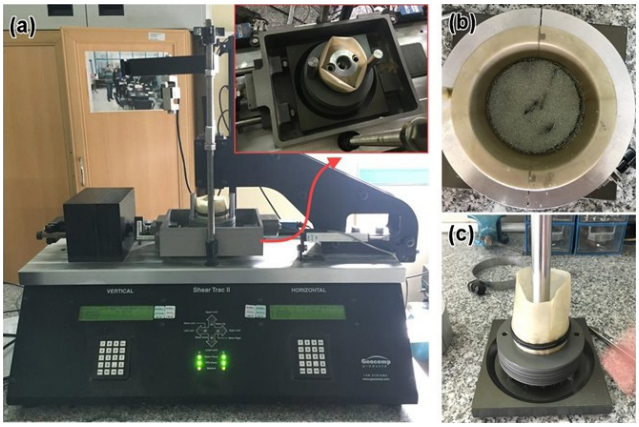

Fig. 5 Views from cyclic simple shear test: (a) overall view of the device; (b) specimen preparation; (c) teflon-coated rings surrounding the specimen

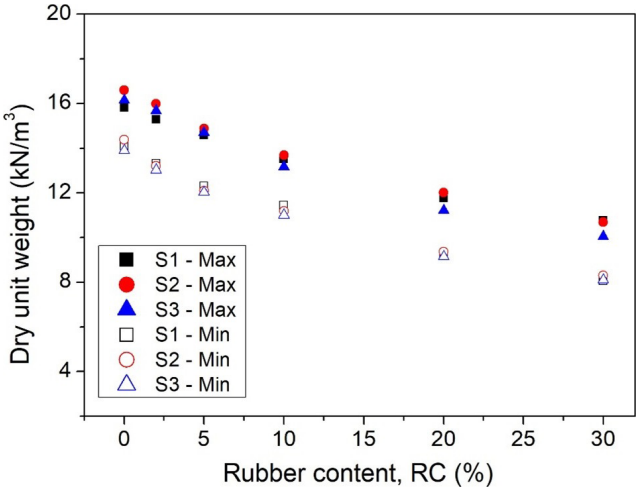

Fig. 6 Variation of maximum and minimum dry unit weights with rubber content

The samples were compressed vertically until a consolidation pressure of 100 kPa was reached before shearing. The horizontal cyclic motion was applied with a frequency of 1.0 Hz. The cyclic shearing was conducted under the constant volume to adopt the undrained conditions by adjusting the magnitude of effective vertical stress [40, 41]. For this purpose, the vertical strain of the samples should be within ±0.05%, as indicated by ASTM D6528-24 [39]. Fig. 7 shows a typical cyclic response obtained for pure S2 sand. The specimen is forced by horizontal sinusoidal loading and the vertical strain is within the required limits during the test.

It can be observed that the effective vertical stress decreases with shaking to comply with the constant volume condition.

Table 4 Program for CBR and cyclic simple shear tests

Test	Sand	Rubber	Purpose of combination	Rubber content (%)
CBR	S2, S3	R1	Sand shape effect	0, 2, 5, 10, 20
	S2	R1, R2	Rubber shape effect	
Cyclic	S1, S2, S3	R1	Sand shape effect	0, 2, 5, 10, 20, 30, 100
	S1	R1, R2	Rubber shape effect	0, 2, 5, 10

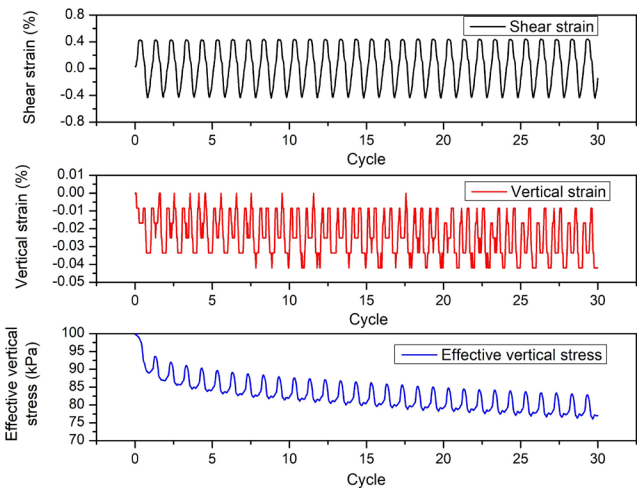

Fig. 7 Cyclic response under constant volume control

5 Results and discussion

5.1 CBR values

The influence of particle shape and deformability on the behavior of the mixtures was first evaluated in terms of bearing capacity under static loading conditions. For this purpose, CBR values were used to interpret the variation of the bearing capacity with the particle shape and rubber content parameters as presented in Fig. 8.

In the evaluation of the sand particle shape effect, R1 rubber was used as an additive for each sand group. For the rubber shape effect, R1 and R2 rubbers were added to S2 sand sample. Due to the high regularity of S1 particles, the cylindrical piston led to the non-uniform settlements in the CBR mold. This caused inconsistent results. Therefore, the effect of sand particle shape for CBR tests was studied using only S2 and S3 sands. Fig. 8 (a) shows that irregular S3 sand with OR = 0.755 produced higher bearing capacities (i.e., CBR) than S2 sand for all rubber content (RC) of mixtures. CBR was 7.2 for pure S3 sand and with the addition of 2% R1 rubber particles, the CBR slightly increased. However, CBR values decreased continuously with the further increase of RC values and reached a value of 1.2 when RC was 20%. On the other hand, for S2 sand, the decreasing trend of CBR values was continuous from RC = 0% to 20%. Another point that draws attention in Fig. 8 (a) is that the effect of the sand particle shape disappears with increasing RC and the CBR values become equal at RC = 20% for S2 and S3 sands. Fig. 8 (b) shows the effect of rubber particle shape on the bearing capacity of the mixtures. For all rubber contents, elongated R2 rubber with OR = 0.564 produced higher CBR values than R1 rubber with OR = 0.749. When R2 rubber with RC = 2% added to S2 sand, CBR increased from 6.5 to 7.2. However, as RC reached 20%, CBR steadily declined to 1.7. On the other hand, the addition of R1 rubber resulted in a constant decrease in CBR with increasing rubber content.

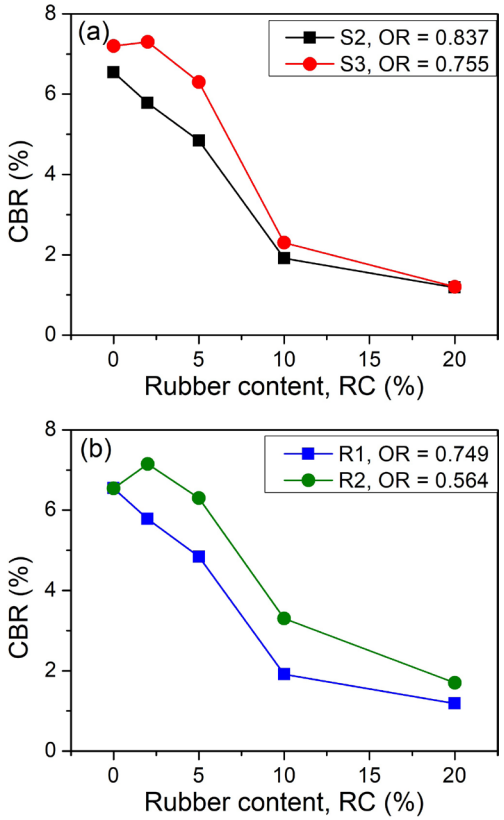

Fig. 8 Variation of CBR with rubber content for: (a) sand; (b) rubber particle shape effect

The CBR test reveals that the bearing capacities decrease with increasing OR of the particles for both sand and rubber particles. The response of pure sand shows that the interlocking mechanism developed between irregular sand particles leads to a higher bearing capacity in S3 than in S2 sand. For irregular S3 sand, the addition of R1 rubber particles at relatively small amounts can improve the bearing capacity of the mixtures. However, this effect is not the case for more regular S2 sand. When elongated R2 particles are used instead of crumb R1 particles, an improvement in the bearing capacity of S2 sand can also occur for a limited amount of the rubber. At high rubber contents, significant reductions in the bearing capacities occur, regardless of the particle shape of the sand and rubber, since the soft structure of the rubber particles dominates the mechanical response of the mixtures.

5.2 Cyclic simple shear test results

Fig. 9 shows the typical hysteresis loops for S1, S2, and S3 sand mixtures with respect to shear strain (γ) level. The loops correspond to the last cyclic of the loads. It is obvious that the particle shape and rubber content affect the hysteresis behavior of the sand-rubber mixtures. In pure sand sample (i.e., RC = 0%), the loop exhibits an anti-S-shaped form. This form disappears gradually with the increase of rubber content. Finally, in the pure rubber sample (i.e., RC = 100%), the hysteresis loops take on a more regular shape, especially at higher strain levels (i.e., γ = 1.3 and 3.0). The maximum shear stress for the same strain level increases with the irregularity of the sand particles.

Fig. 10 illustrates the variation of the equivalent excess pore-water pressure ratio (r_u) with the number of cycles (N) for the boundary strain levels (0.2% and 3.0%). Within the dry, constant-volume (NGI-type) framework, r_u is derived from the degradation of the vertical effective stress as:

$$r_u = 1 - \left(\sigma'_v / \sigma'_{v,0}\right).$$

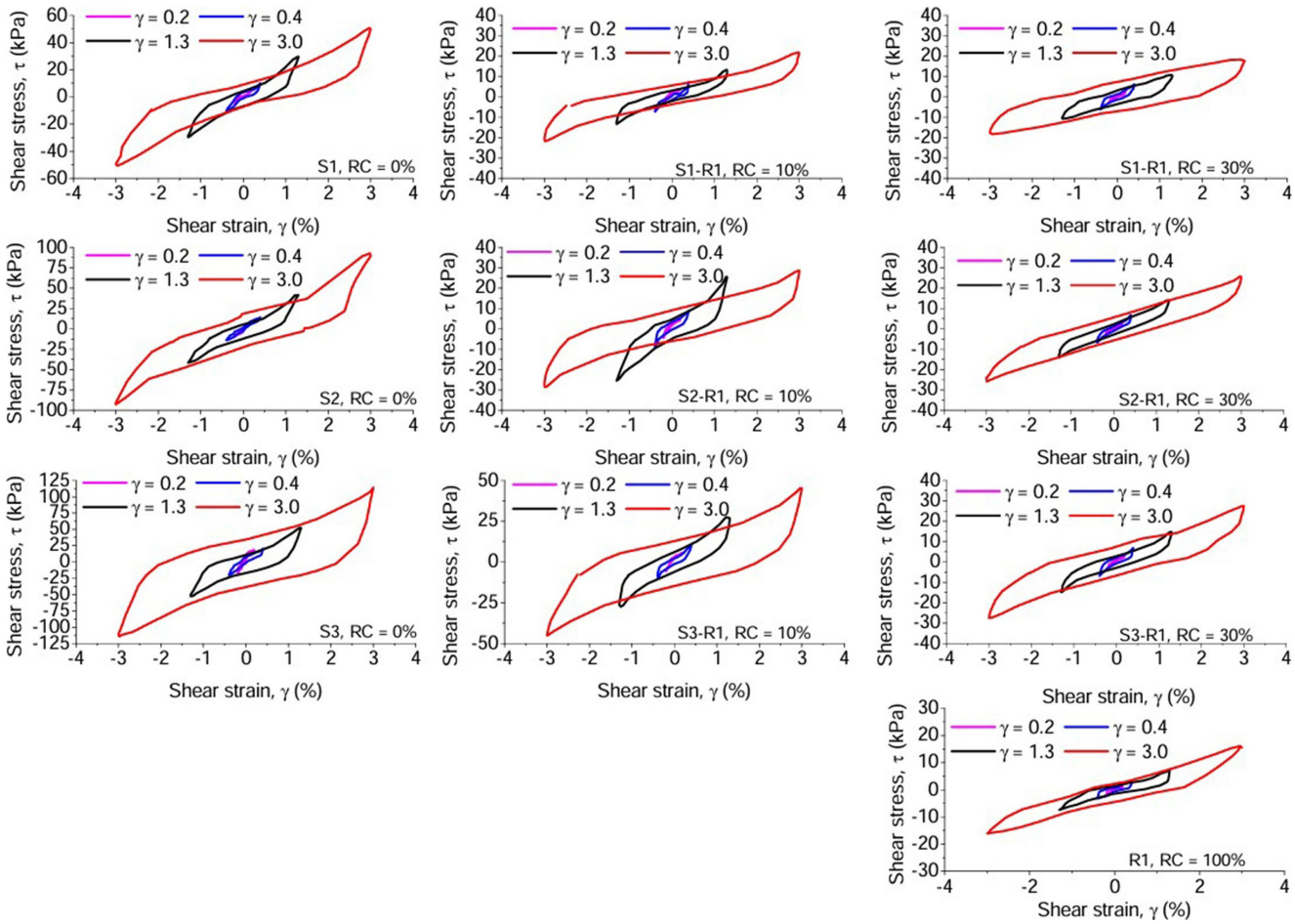

Fig. 9 Typical hysteresis plots of S1, S2, and S3 mixtures with respect to strain level

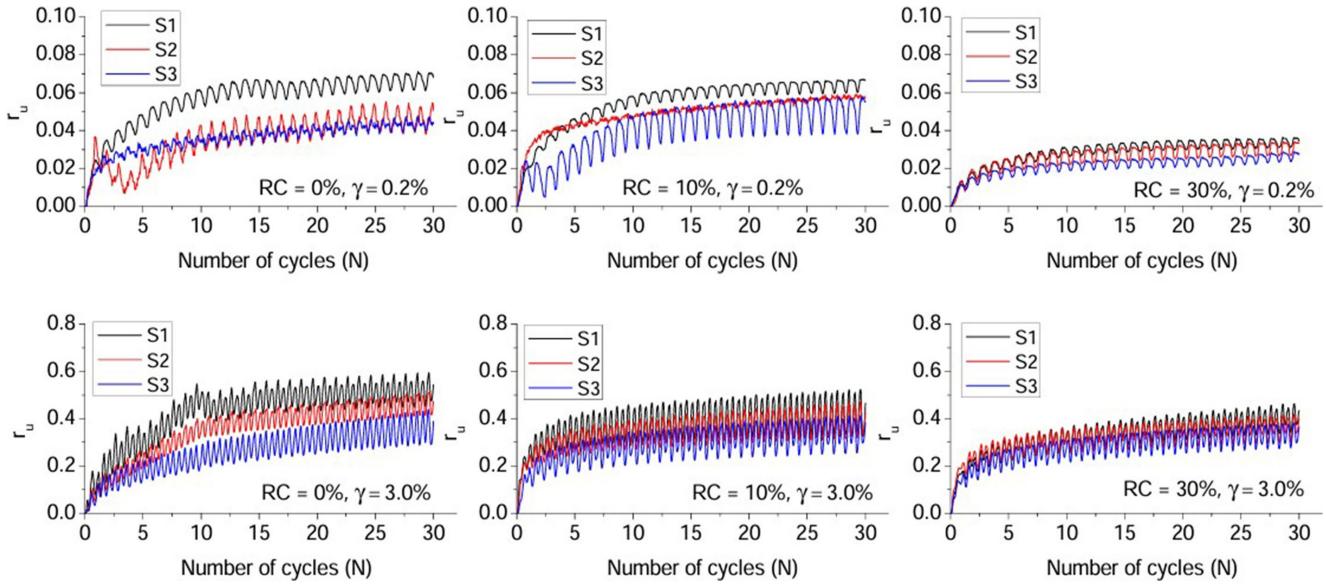

Fig. 10 Variation of equivalent excess pore water pressures

As shown in Fig. 10, all specimens remained in the pre-failure or pre-liquefaction zone (r_u < 1.0) throughout the 30-cycle duration, even at the maximum target strain of 3.0%. This stability confirms that the specimens maintained their fabric integrity, allowing for a reliable characterization of secant shear modulus and damping ratio.

Fig. 10 indicates that the generation of r_u is affected by both particle shape and rubber content. As the Overall

Regularity (OR) of the sand particles increases, the samples tend to generate higher r_u values. In other words, the rate of decrease in effective vertical stress is promoted with the regular particles. Therefore, S1 sand with the highest OR = 0.904 produced the highest r_u values, while S3 sample with the lowest OR = 0.756 generated the lowest r_u values. On the other hand, with the addition of rubber particles, the increase of r_u was slowed and the lowest values were obtained at RC = 30%. In addition, the influence of sand particle shape was weakened with the increase of rubber content.

5.2.1 Shear modulus

The shear modulus of the samples was calculated using secant shear modulus term (G_{sec}) described in Vucetic and Dobry [42]. The secant shear modulus corresponds to the slope of line joining the maximum and minimum points of a hysteresis loop. The mean G_{sec} of the last ten cycles was used to obtain a representative G_{sec} for each test. Fig. 11 shows the effect of sand particle shape on G_{sec} of the mixtures at different shear strain level. In Fig. 11, the G_{sec} of pure sand and rubber materials is also presented. First of all, it can be observed that the G_{sec} gradually decreases with the increase of shear strain for all cases. This decrease is more evident in irregular S3 (i.e., OR = 0.755) pure sand than in regular S1 (i.e., OR = 0.908) pure sand. The effects of sand particle shape on the G_{sec} are completely strain- and rubber content- dependent.

The G_{sec} decreases with increasing OR, and this trend can be clearly observed at relatively small-strain levels (i.e., Fig. 11 (a) and (b)). At γ = 0.2% and 0.4% strains, the addition of RC = 2% rubber particles led to a decrease in G_{sec} of S1 sand, while it caused an improvement of G_{sec} of S2 and S3 sands. This improvement was more apparent in the S3 sand. A similar improvement effect was also detected in the CBR response of S3 sand. This response can be clarified by interpreting the relationship between the void ratio and rubber particle role in the mixtures. As it has been emphasized in previous studies, the regular particles tend to form a dense granular structure; therefore, the void ratios are higher in the irregular samples [10, 43]. This is why the rubber particles have more chance to fill the voids and support the force columns in the irregular sand samples [44]. This may be the reason for the increase in G_{sec} of S2 and S3 sands with RC = 2% rubber addition. However, with the increase of RC and shear strain, the supporting role of rubber particles disappears, and rubber particles begin to take a primary role in the force chains. To interpret the role of rubber particles in the mixture, the samples were imaged using a transparent

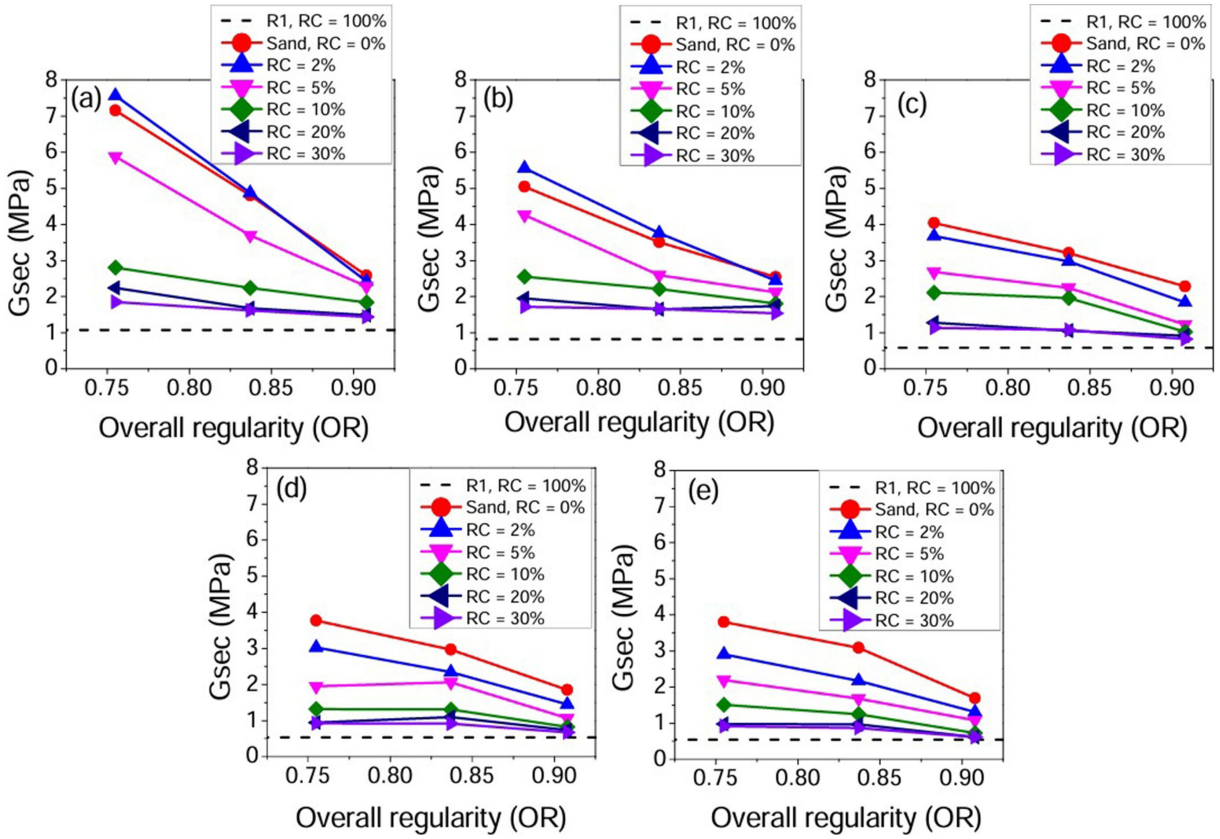

Fig. 11 Variation of G_{sec} with sand particle shape effect at different shear strain level: (a) γ = 0.2%; (b) γ = 0.4%; (c) γ = 1.3%; (d) γ = 2.0%; (e) γ = 3.0%

box for the cases of RC = 0%, 2%, and 20%, as shown in Fig. 12. S2 and R1 particles were used for this purpose. Fig. 12 (a) shows that the force columns consist only of rigid sand particles in the case of pure sand. When the rubber particles with RC = 2% are added into the sand, the primary force chains formed by the sand particles are supported by rubber particles, and the rubber particles act as secondary particles to prevent the bucking of the primary force chains (i.e., Fig. 12 (b)). However, as the rubber content increases to RC = 20%, the primary force chains consist mostly of soft rubber particles (i.e., Fig. 12 (c)). Consequently, the G_{sec} decreases with the increase of RC due to the soft nature of the rubber particles.

Fig. 13 shows the effect of rubber shape on the G_{sec} of S1 mixtures. The elongated R2 rubber (OR = 0.564) led to a higher G_{sec} than crumb R1 rubber (OR = 0.749) in all RC and strain conditions. This trend can be explained by the distribution of contacts between sand and rubber particles. Fig. 14 shows the variation of contact numbers between sand and rubber particles depending on the rubber particle shape. It is seen that R1 rubber (i.e., Fig. 14 (a)) produces smaller contact numbers than R2 rubber (i.e., Fig. 14 (b)). The inter-particle friction capacity of R2 mixtures is higher than R1 mixtures and R2 rubbers produce higher G_{sec} than R1. The notable point from Fig. 13 is the improvement effect of R2 rubber. For RC = 2%, the S1-R2 mixtures produced higher G_{sec} than S1 pure sand for all strain cases. However, the level of improvement decays with increasing strain level. When RC was increased G_{sec} experienced a decrease in both shape characteristics and the improvement effect of R2 vanished.

5.2.2 Damping ratio

Fig. 15 presents the effect of sand particle shape on the damping ratio of the mixtures. Fig. 15 points that the effect of particle shape needs to be associated with the rubber content and strain level parameters. First of all, it can be observed that the damping ratio increases with the shear strain level. However, the variation rate differs with respect to the soft rubber content. While the damping ratio

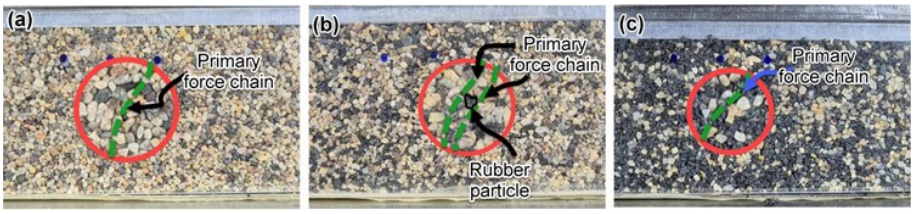

Fig. 12 Role of sand and rubber particles in mixtures: (a) RC = 0%; (b) RC = 2%; (c) RC = 20%

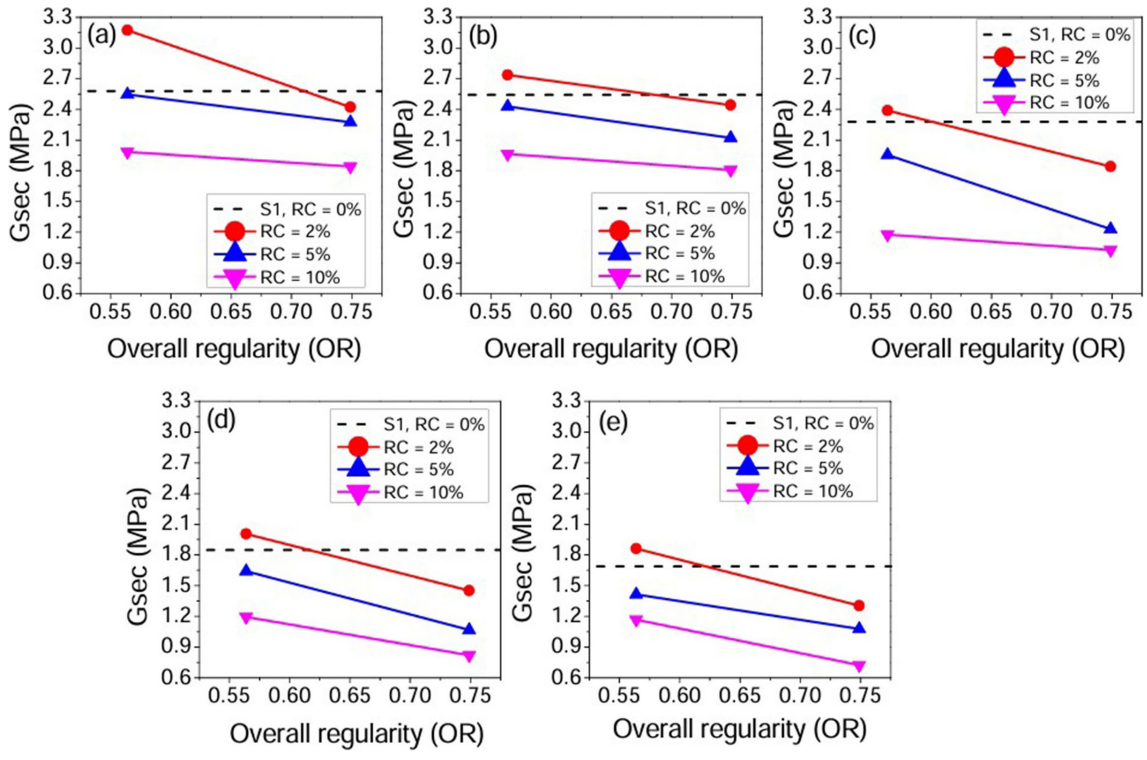

Fig. 13 Variation of G_{sec} with rubber particle shape effect at different shear strain level: (a) γ = 0.2%; (b) γ = 0.4%; (c) γ = 1.3%; (d) γ = 2.0%; (e) γ = 3.0%

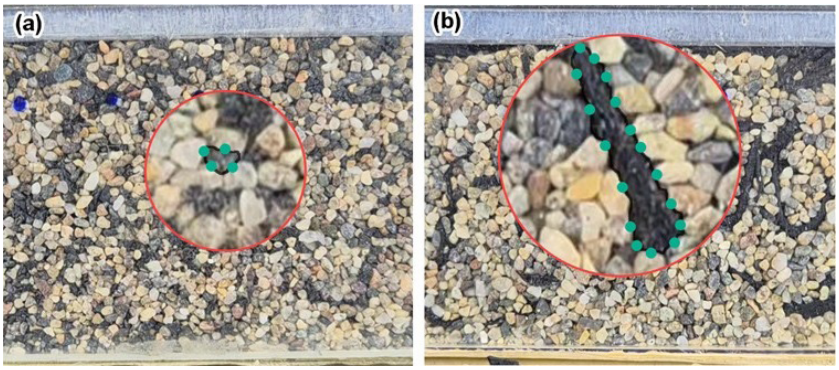

Fig. 14 Interaction of sand and rubber particles in: (a) R1 and (b) R2 mixtures (note: each contact between sand and rubber particles is indicated with a circle)

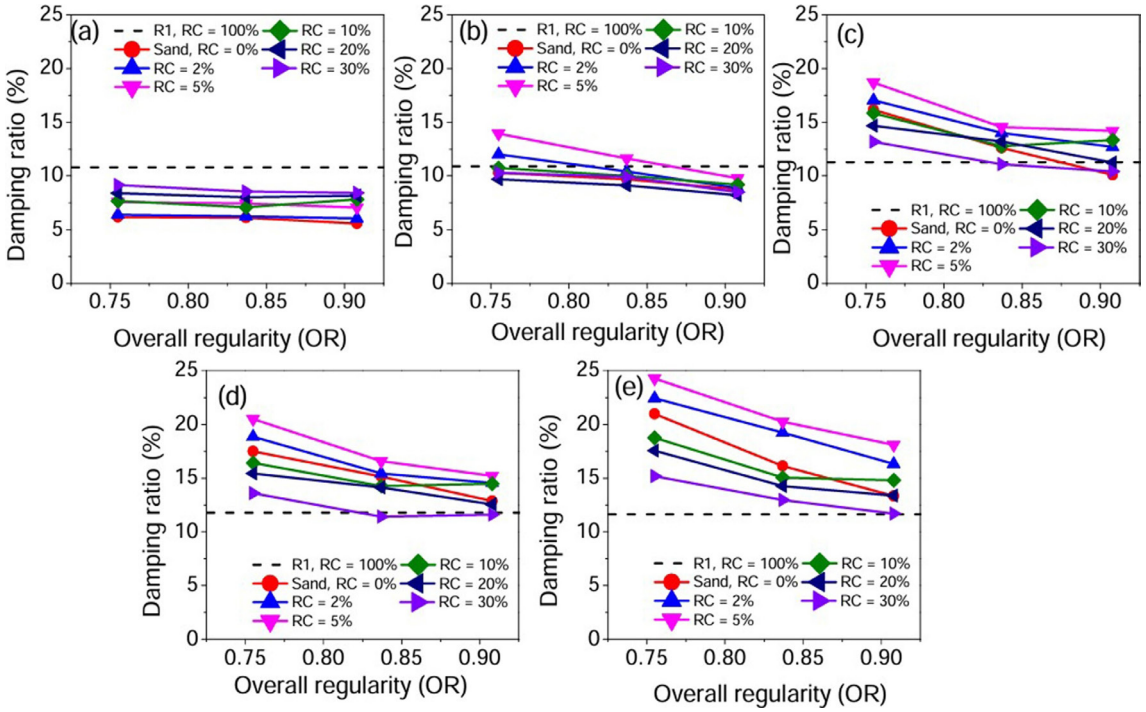

Fig. 15 Variation of damping ratio with sand particle shape effect at different shear strain level: (a) γ = 0.2%; (b) γ = 0.4%; (c) γ = 1.3%; (d) γ = 2.0%; (e) γ = 3.0%

increases significantly with shear strain in pure sand material (i.e., RC = 0%), the increase rate in pure rubber (i.e., RC = 100%) is quite low.

At γ = 0.2%, the highest damping ratio was observed in pure R1 rubber (i.e., RC = 100%) and pure sand materials (i.e., RC = 0%) have the lowest damping content. At this strain level, the effect of sand particle shape is ambiguous. When the strain level is raised to γ = 0.4%, the particle shape effect appears in the mixtures. The damping ratio enhances with the decrease of OR. In other words, the irregular particles promote the damping ratio more than the regular particles.

When pure sand material is considered as reference, there is an optimum situation in the change of damping ratio in terms of the RC effect. The damping ratio increased with rubber content up to RC = 5% and showed a decreasing trend for further rubber contents. At a shear strain of γ = 0.4% (i.e., Fig. 15 (b)), the damping ratio of RC = 100% was exceeded in the cases of S2, RC = 5%; S3, RC = 5% and 2%. As strain reached γ = 2.0%, the damping ratio of RC = 100% was exceeded by almost all mixtures. The RC = 5% and RC = 2% mixtures of S2 and S3 sands maintain their superiority over pure sands for the strains between γ = 0.4% and γ = 3.0%. The trend of damping ratio with respect to particle shape, shear strain and rubber content can be reasoned by reviewing the content of the damping energy.

The energy dissipation in granular medium occurs in two different ways:

1. Frictional (i.e., interparticle sliding, rotation, interlocking and translation);
2. Particle deformation and particle breakage [16, 45].

Since the normal stress (100 kPa) is relatively low to cause measurable grain breakage, the sands are considered sufficiently rigid to resist breakage during testing. Therefore, it is considered that energy can only be dissipated by the first mechanism, and the effect of sand particle shape on the damping ratio can be evaluated by focusing on frictional damping. This frictional mechanism inherently involves micro-scale abrasion and the abrasion of surface asperities at contact points [46].

As shown in Fig. 15, the sand particle shape effect becomes more obvious with the increase of shear strain. This is because particle kinematics are activated by shear strain and shape properties exert their influence on frictional damping.

Since the interparticle friction coefficient of the elastic rubber is relatively high, the energy dissipation is accomplished by the particle deformation under shear strain. This is why, at relatively small strain (i.e., Fig. 15 (a)), the pure rubber material produced higher damping than other cases, and the damping ratio of pure rubber changed little even if the strain level increased significantly in Fig. 15 (b) to (e). However, in mixed granular system, both friction and particle deformation mechanisms contribute to the damping [47, 48]. An optimum situation in terms of damping ratio emerges as a result of the friction and deformation contribution of sand and rubber particles, respectively. Therefore, the damping ratio increased as the addition of rubber up to 5% provided damping through particle deformation without damaging the particle kinematics. However, further increase of RC weakened the friction mechanism in mixtures and accordingly the damping ratio decreased at large strain levels.

Fig. 16 shows the effect of rubber particle shape on the damping ratio. R1 and R2 rubber particles produced similar damping ratios at relatively small strain levels (Fig. 16 (a) and (b)). With the increase of shear strain, the particle shape effect appeared in the mixtures (Fig. 16 (c) to (e)). The R2 elongated rubber led to a higher damping than R1 crumb rubber. Fig. 17 shows the evolution of R2 form with the effect of shear strain. As mentioned in Fonseca et al. [49], the elongated rubber particles have the ability to wrap the sand particles. Therefore, elongated rubbers produce higher contact numbers than crumb particles and behave like a fiber at large strain levels. This property of R2 rubber provides higher deformability compared to crumb R1 under similar loading conditions. The increase in damping ratio as OR decreases can be clarified by considering the fiber effect and contact number characteristic of elongated R2 rubber particles.

6 Conclusions

In this study, the combined roles of particle shape and deformability on the cyclic response of the sand-rubber mixtures were examined through cyclic simple shear tests.

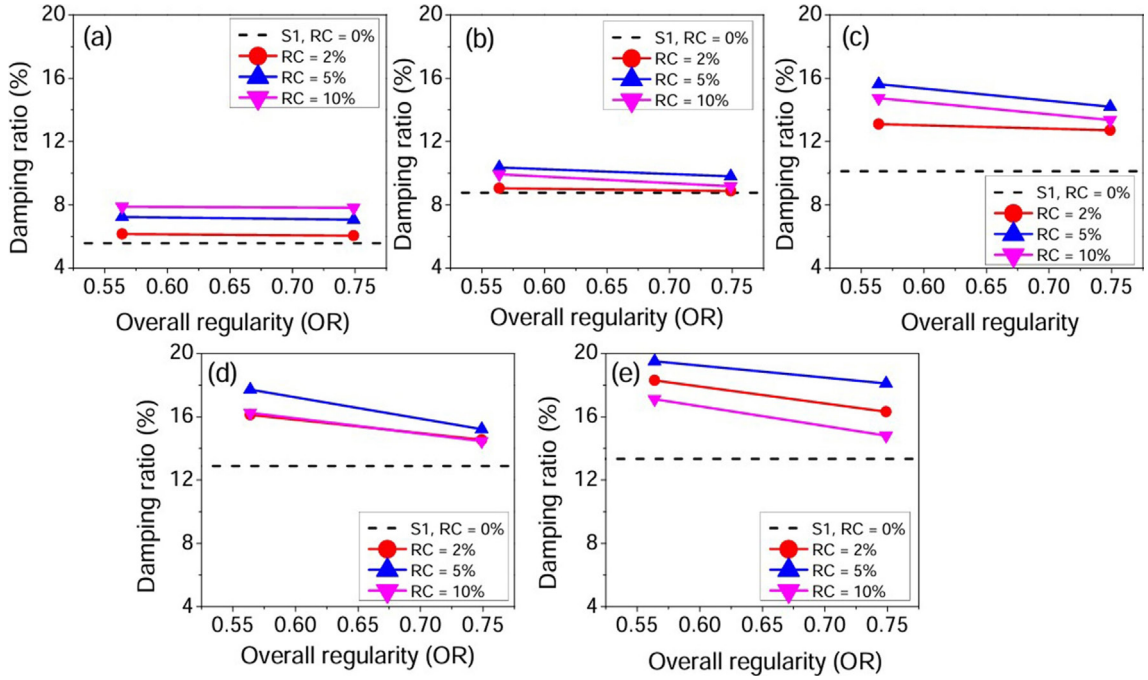

Fig. 16 Variation of damping ratio with rubber particle shape effect at different shear strain level: (a) $\gamma = 0.2\%$; (b) $\gamma = 0.4\%$; (c) $\gamma = 1.3\%$; (d) $\gamma = 2.0\%$; (e) $\gamma = 3.0\%$

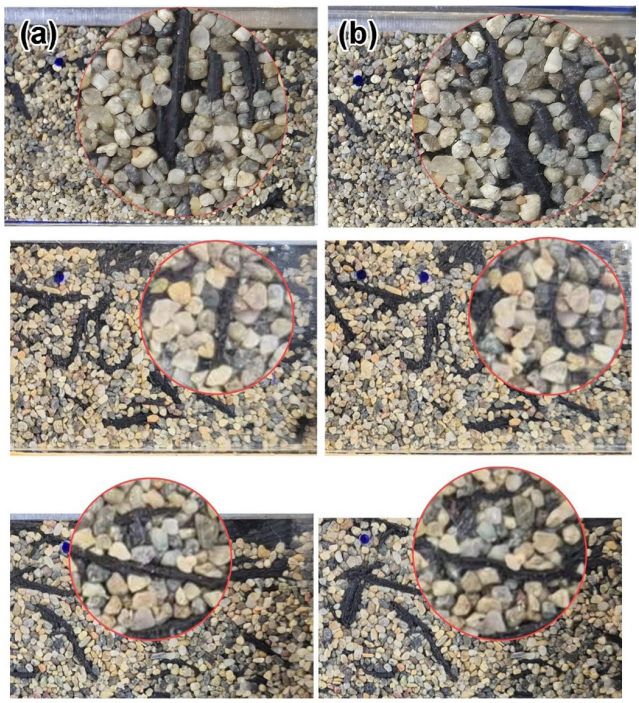

Fig. 17 Transformation of R2 rubber form: (a) before shearing; (b) after shearing

In order to gain comprehensive insight into the geotechnical response, the static response of the mixtures was also included using California bearing ratio (CBR) tests. In addition, the role of rubber particle shape and content was elaborated using the local image of the samples through transparent shear box. Overall, the following outcomes were produced from this study:

1. The CBR values increase with decreasing OR of the sand particles. However, the influence of sand morphology on the CBR values becomes negligible as the concentration of rubber increases.
2. The CBR values decrease with increasing OR of the rubber particles. In other words, the elongated rubber particles produced higher bearing capacities than the crumb rubber.
3. The interactive role of particle shape and rubber content can be observed at smaller rubber contents. Addition of 2% rubber particles improves the CBR of irregular S3 sand, while it leads to a decrease in the CBR of S2 sand. Meanwhile, the elongated R2 particles with 2% content provides an increase in the bearing capacity, contrary to the effect of R1 particles. For higher rubber contents, CBR values decrease with increasing rubber content, regardless of particle shape characteristics.
4. The shear modulus decreases with increasing OR of sands. The effects of sand particle shape on the shear modulus are strain- and rubber content- dependent. At relatively small-strain levels, the addition of RC = 2% rubber particles leads to a decrease in G_{sec} of S1 sand, while it provides an improvement for S2 and S3 sands. The level of improvement enhances as the particles became more irregular. A similar effect is also detected in the CBR values.
5. The shear modulus increases with decreasing OR of rubber particles. For all shear strain levels, the addition of 2% rubber with R2 shape produced an improvement in the G_{sec}. The level of improvement decreases as the shear strain level increases.
6. At the small-strain levels, the soft rubber particles produce higher damping ratio than the rigid sand particles and the effect of sand particle shape is uncertain. The damping ratio of pure sand exceeds the damping ratio of the pure rubber at the large-strain levels. The effect of sand particle shape appears with the increase of shear strain level. The decrease in OR of sand results in an increase in the damping ratio.
7. Considering the damping ratio of pure sands as reference, the addition of rubber particles up to RC = 5% results in an increase in the damping ratio of mixtures between medium and large strain levels.
8. The decrease in OR of rubber particles increases the damping ratio. The effect of rubber particle shape occurs with increasing shear strain.

Ultimately, the findings confirm that the cyclic behavior of sand-rubber composites is governed by a complex interplay between particle morphology and deformability. The evolution of both the secant shear modulus and damping ratio reflects the significance of these physical attributes in modulating the material's dynamic response. In future work, the effects of particle shape and deformability on the dynamic properties can be elaborated for various strain ranges using different testing methods. In addition, investigations including microscale responses will disclose the interaction mechanism of particles; thus, the variation of dynamic properties can be clearly reasoned in terms of particle shape and deformability influences.

References

[1] Zhou, B., Wang, J., Zhao, B. "Micromorphology characterization and reconstruction of sand particles using micro X-ray tomography and spherical harmonics", Engineering Geology, 184, pp. 126–137, 2015. https://doi.org/10.1016/j.enggeo.2014.11.009

[2] Sadrekarimi, A., Olson, S. M. "Critical state friction angle of sands", Géotechnique, 61(9), pp. 771–783, 2011. https://doi.org/10.1680/geot.9.P.090

[3] Ari, A., Akbulut, S. "Effect of particle size and shape on shear strength of sand–rubber granule mixtures", Granular Matter, 24(4), 126, 2022. https://doi.org/10.1007/s10035-022-01287-7

[4] Madhusudhan, B. R., Boominathan, A., Banerjee, S. "Cyclic Simple Shear Response of Sand–Rubber Tire Chip Mixtures", International Journal of Geomechanics, 20(9), 04020136, 2020. https://doi.org/10.1061/(ASCE)GM.1943-5622.0001761

[5] Rios, S., Kowalska, M., Viana da Fonseca, A. "Cyclic and Dynamic Behavior of Sand–Rubber and Clay–Rubber Mixtures", Geotechnical and Geological Engineering, 39(5), pp. 3449–3467, 2021. https://doi.org/10.1007/s10706-021-01704-3

[6] Anastasiadis, A., Senetakis, K., Pitilakis, K. "Small-Strain Shear Modulus and Damping Ratio of Sand-Rubber and Gravel-Rubber Mixtures", Geotechnical and Geological Engineering, 30(2), pp. 363–382, 2012. https://doi.org/10.1007/s10706-011-9473-2

[7] Peña, A. A., García-Rojo, R., Herrmann, H. J. "Influence of particle shape on sheared dense granular media", Granular Matter, 9(3), pp. 279–291, 2007. https://doi.org/10.1007/s10035-007-0038-2

[8] Wu, Y., Cui, J., Huang, J., Zhang, W., Yoshimoto, N., Wen, L. "Correlation of Critical State Strength Properties with Particle Shape and Surface Fractal Dimension of Clinker Ash", International Journal of Geomechanics, 21(6), 04021071, 2021. https://doi.org/10.1061/(ASCE)GM.1943-5622.0002027

[9] Lashkari, A., Falsafizadeh, S. R., Shourijeh, P. T., Alipour, M. J. "Instability of loose sand in constant volume direct simple shear tests in relation to particle shape", Acta Geotechnica, 15(9), pp. 2507–2527, 2020. https://doi.org/10.1007/s11440-019-00909-4

[10] Shin, H., Santamarina, J. C. "Role of Particle Angularity on the Mechanical Behavior of Granular Mixtures", Journal of Geotechnical and Geoenvironmental Engineering, 139(2), pp. 353–355, 2013. https://doi.org/10.1061/(ASCE)GT.1943-5606.0000768

[11] Ha Giang, P. H., Van Impe, P. O., Van Impe, W. F., Menge, P., Haegeman, W. "Small-strain shear modulus of calcareous sand and its dependence on particle characteristics and gradation", Soil Dynamics and Earthquake Engineering, 100, pp. 371–379, 2017. https://doi.org/10.1016/j.soildyn.2017.06.016

[12] Sarkar, D., Goudarzy, M., Wichtmann, T. "Inspection of various grain morphology parameters based on wave velocity measurements on three different granular materials", Soil Dynamics and Earthquake Engineering, 153, 107071, 2022. https://doi.org/10.1016/j.soildyn.2021.107071

[13] Ahmed, S. S., Martinez, A. "Effects of Particle Shape on the Shear Wave Velocity and Shear Modulus of 3D Printed Sand Analogs", Open Geomechanics, 3, 1, 2022. https://doi.org/10.5802/ogeo.9

[14] Hu, J., Wu, H., Gu, X., Zhou, Q. "Particle shape effects on dynamic properties of granular soils: A DEM study", Computers and Geotechnics, 161, 105578, 2023. https://doi.org/10.1016/j.compgeo.2023.105578

[15] Nakhaei, A., Marandi, S. M., Sani Kermani, S., Bagheripour, M. H. "Dynamic properties of granular soils mixed with granulated rubber", Soil Dynamics and Earthquake Engineering, 43, pp. 124–132, 2012. https://doi.org/10.1016/j.soildyn.2012.07.026

[16] Feng, Z.-Y., Sutter, K. G. "Dynamic Properties of Granulated Rubber/Sand Mixtures", Geotechnical Testing Journal, 23(3), pp. 338–344, 2000. https://doi.org/10.1520/gtj11055j

[17] Madhusudhan, B. R., Boominathan, A., Banerjee, S. "Static and Large-Strain Dynamic Properties of Sand–Rubber Tire Shred Mixtures", Journal of Materials in Civil Engineering, 29(10), 04017165, 2017. https://doi.org/10.1061/(ASCE)MT.1943-5533.0002016

[18] Madhusudhan, B. R., Boominathan, A., Banerjee, S. "Factors Affecting Strength and Stiffness of Dry Sand-Rubber Tire Shred Mixtures", Geotechnical and Geological Engineering, 37(4), pp. 2763–2780, 2019. https://doi.org/10.1007/s10706-018-00792-y

[19] Liu, F., Zheng, K., Jia, B., Yang, J., Wu, M. "Shear modulus and damping ratio of granulated rubber-sand mixtures: Influence of relative particle size", Construction and Building Materials, 427, 136205, 2024. https://doi.org/10.1016/j.conbuildmat.2024.136205

[20] Edinçliler, A., Yildiz, O. "Effects of processing type on shear modulus and damping ratio of waste tire-sand mixtures", Geosynthetics International, 29(4), pp. 389–408, 2022. https://doi.org/10.1680/jgein.21.00008a

[21] ASTM International "ASTM D854-23 Standard Test Methods for Specific Gravity of Soil Solids by the Water Displacement Method", ASTM International, West Conshohocken, PA, USA, 2023. https://doi.org/10.1520/D0854-23

[22] ASTM International "ASTM D698-12 Standard Test Methods for Laboratory Compaction Characteristics of Soil Using Standard Effort (12 400 ft-lbf/ft^3 (600 kN-m/m^3))", ASTM International, West Conshohocken, PA, USA, 2012. https://doi.org/10.1520/D0698-12

[23] Yang, J., Luo, X. D. "Exploring the relationship between critical state and particle shape for granular materials", Journal of the Mechanics and Physics of Solids, 84, pp. 196–213, 2015. https://doi.org/10.1016/j.jmps.2015.08.001

[24] Ari, A., Akbulut, S. "Evaluation of sand–geomembrane interface behavior using discrete element method", Granular Matter, 24(1), 21, 2022. https://doi.org/10.1007/s10035-021-01183-6

[25] Barrett, P. J. "The shape of rock particles, a critical review", Sedimentology, 27(3), pp. 291–303, 1980. https://doi.org/10.1111/j.1365-3091.1980.tb01179.x

[26] Blott, S. J., Pye, K. "Particle shape: a review and new methods of characterization and classification", Sedimentology, 55(1), pp. 31–63, 2008. https://doi.org/10.1111/j.1365-3091.2007.00892.x

[27] Altuhafi, F., O'Sullivan, C., Cavarretta, I. "Analysis of an Image-Based Method to Quantify the Size and Shape of Sand Particles", Journal of Geotechnical and Geoenvironmental Engineering, 139(8), pp. 1290–1307, 2013. https://doi.org/10.1061/(asce)gt.1943-5606.0000855

[28] Fonseca, J., O'Sullivan, C. "A re-evaluation of the Fourier descriptor approach to quantifying sand particle geometry", In: 4th International Symposium on Deformation Characteristics of Geomaterials, Atlanta, GA, USA, 2008, pp. 687–690. ISBN 1586039083

[29] Kootahi, K., Leung, A. K., Wang, Y. "Modified value stabilization methodology (MVSM) to efficiently determine the sample size required for particle morphology quantification", Powder Technology, 420, 118396, 2023. https://doi.org/10.1016/j.powtec.2023.118396

[30] Schneider, C. A., Rasband, W. S., Eliceiri, K. W. "NIH Image to ImageJ: 25 years of image analysis", Nature Methods, 9(7), pp. 671–675, 2012. https://doi.org/10.1038/nmeth.2089

[31] Abràmoff, M. D., Magalhães, P. J., Ram, S. J. "Image Processing with ImageJ", [pdf] Biophotonics International, 2004. Available at: https://imagej.net/ij/docs/pdfs/Image_Processing_with_ImageJ.pdf [Accessed: 30 July 2025]

[32] ASTM International "ASTM D1883-21 Standard Test Method for California Bearing Ratio (CBR) of Laboratory-Compacted Soils", ASTM International, West Conshohocken, PA, USA, 2021. https://doi.org/10.1520/D1883-21

[33] Wichtmann, T., Triantafyllidis, T. "Influence of the Grain-Size Distribution Curve of Quartz Sand on the Small Strain Shear Modulus G_{max}", Journal of Geotechnical and Geoenvironmental Engineering, 135(10), pp. 1404–1418, 2009. https://doi.org/10.1061/(ASCE)GT.1943-5606.0000096

[34] Rui, S., Guo, Z., Si, T., Li, Y. "Effect of particle shape on the liquefaction resistance of calcareous sands", Soil Dynamics and Earthquake Engineering, 137, 106302, 2020. https://doi.org/10.1016/j.soildyn.2020.106302

[35] Bjerrum, L., Landva, A. "Direct Simple-Shear Tests on a Norwegian Quick Clay", Géotechnique, 16(1), pp. 1–20, 1966. https://doi.org/10.1680/geot.1966.16.1.1

[36] Nong, Z.-Z., Park, S.-S., Lee, D.-E. "Comparison of sand liquefaction in cyclic triaxial and simple shear tests", Soils and Foundations, 61(4), pp. 1071–1085, 2021. https://doi.org/10.1016/j.sandf.2021.05.002

[37] Sivathayalan, S., Ha, D. "Effect of static shear stress on the cyclic resistance of sands in simple shear loading", Canadian Geotechnical Journal, 48(10), pp. 1471–1484, 2011. https://doi.org/10.1139/t11-056

[38] ASTM International "ASTM D4254-00 Standard Test Methods for Minimum Index Density and Unit Weight of Soils and Calculation of Relative Density", ASTM International, West Conshohocken, PA, USA, 2017. https://doi.org/10.1520/D4254-00

[39] ASTM International "ASTM D6528-24 Standard Test Method for Consolidated Undrained Direct Simple Shear Testing of Fine-Grained Soils", ASTM International, West Conshohocken, PA, USA, 2024. https://doi.org/10.1520/D6528-24

[40] Reyno, A. J., Airey, D., Taiebat, H. "Influence of height and boundary conditions in simple shear tests", in: Frontiers in Offshore Geotechnics, Taylor & Francis, 2005, pp. 1101–1107. ISBN 978-0-415-88934-6 https://doi.org/10.1201/NOE0415390637.ch134

[41] Dyvik, R., Berre, T., Lacasse, S., Raadim, B. "Comparison of truly undrained and constant volume direct simple shear tests", Géotechnique, 37(1), pp. 3–10, 1987. https://doi.org/10.1680/geot.1987.37.1.3

[42] Vucetic, M., Dobry, R. "Degradation of Marine Clays under Cyclic Loading", Journal of Geotechnical Engineering, 114(2), pp. 133–149, 1988. https://doi.org/10.1061/(ASCE)0733-9410(1988)114:2(133)

[43] Ari, A., Akbulut, S. "Investigation of micro-scale shear response of sand–rubber granule mixture in terms of particle shape and grain scale deformability effects", Particuology, 90, pp. 452–469, 2024. https://doi.org/10.1016/j.partic.2024.01.013

[44] Lee, J.-S., Dodds, J., Santamarina, J. C. "Behavior of Rigid-Soft Particle Mixtures", Journal of Materials in Civil Engineering, 19(2), pp. 179–184, 2007. https://doi.org/10.1061/(ASCE)0899-1561(2007)19:2(179)

[45] Xiao, Y., Yuan, Z., Chu, J., Liu, H., Huang, J., Luo, S. N., Wang, S., Lin, J. "Particle breakage and energy dissipation of carbonate sands under quasi-static and dynamic compression", Acta Geotechnica, 14(6), pp. 1741–1755, 2019. https://doi.org/10.1007/s11440-019-00790-1

[46] Gluchowski, A., Iskander, M. "Evolution of particle breakage during cyclic shear of sand", Granular Matter, 27(3), 76, 2025. https://doi.org/10.1007/s10035-025-01548-1

[47] Santamarina, J. C., Klein, A., Fam, M. A. "Soils and Waves: Particulate Materials Behavior, Characterization and Process Monitoring", Journal of Soils and Sediments, 1(2), p. 130, 2001. https://doi.org/10.1007/BF02987719

[48] Pamukcu, S., Akbulut, S. "Thermoelastic Enhancement of Damping of Sand Using Synthetic Ground Rubber", Journal of Geotechnical and Geoenvironmental Engineering, 132(4), pp. 501–510, 2006. https://doi.org/10.1061/(asce)1090-0241(2006)132:4(501)

[49] Fonseca, J., Riaz, A., Bernal-Sanchez, J., Barreto, D., McDougall, J., Miranda-Manzanares, M., Marinelli, A., Dimitriadi, V. "Particle–scale interactions and energy dissipation mechanisms in sand–rubber mixtures", Géotechnique Letters, 9(4), pp. 263–268, 2019. https://doi.org/10.1680/jgele.18.00221